Heme Redox Potential Control in de Novo Designed Four-α-Helix Bundle Proteins[†]

Julia M. Shifman,[‡] Brian R. Gibney,[§] R. Eryl Sharp, and P. Leslie Dutton*

The Johnson Research Foundation, Department of Biochemistry and Biophysics, University of Pennsylvania, Philadelphia, Pennsylvania 19104

ABSTRACT: The effects of various mechanisms of metalloporphyrin reduction potential modulation were investigated experimentally using a robust, well-characterized heme protein maquette, synthetic protein scaffold H10A24 [{CH_3CONH-CGGGELWKL·HEELLKK·FEELLKL·AEERLKK·L-$CONH_2$}$_2$]$_2$. Removal of the iron porphyrin macrocycle from the high dielectric aqueous environment and sequestration within the hydrophobic core of the H10A24 maquette raises the equilibrium reduction midpoint potential by 36−138 mV depending on the hydrophobicity of the metalloporphyrin structure. By incorporating various natural and synthetic metalloporphyrins into a single protein scaffold, we demonstrate a 300-mV range in reduction potential modulation due to the electron-donating/withdrawing character of the peripheral macrocycle substituents. Solution pH is used to modulate the metalloporphyrin reduction potential by 160 mV, regardless of the macrocycle architecture, by controlling the protonation state of the glutamate involved in partial charge compensation of the ferric heme. Attempts to control the reduction potential by inserting charged amino acids into the hydrophobic core at close proximity to the metalloporphyrin lead to varied success, with H10A24-L13E lowering the $E_{m8.5}$ by 40 mV, H10A24-E11Q raising it by 50 mV, and H10A24-L13R remaining surprisingly unaltered. Modifying the charge of the adjacent metalloporphyrin, +1 for iron(III) protoporphyrin IX or neutral for zinc(II) protoporphyrin IX resulted in a loss of 70 mV [Fe(III)PPIX]$^+$ − [Fe(III)PPIX]$^+$ interaction observed in maquettes. Using these factors in combination, we illustrate a 435-mV variation of the metalloporphyrin reduction midpoint potential in a simple heme maquette relative to the about 800-mV range observed for natural cytochromes. Comparison between the reduction potentials of the heme maquettes and other de novo designed heme proteins reveals global trends in the E_m values of synthetic cytochromes.

Redox proteins utilize a relatively small number of cofactors to perform a multitude of tasks. Consequently, it is common for a biological cofactor to display a wide range of redox activity, with each particular cofactor tuned into the range that facilitates protein function. Large variations in cofactor reduction potentials are achieved through a variety of macro- and microenvironmental effects imposed on the redox centers by the surrounding anisotropic protein matrix. Hemes (Fe protoporphyrin IX and its derivatives) form a well-recognized class of biological cofactors that are the functional centers in a family of proteins dominated by the cytochromes. While oxidation/reduction of cytochromes invariably involves a seemingly simple reaction of electron transfer from/to the heme iron, their reduction midpoint potentials span an 800-mV range, from cytochrome c_3 (−400mV vs SHE) to cytochrome b_{559} (+400 mV) (2) (Scheme 1). The modulation of metalloporphyrin reduction potentials is influenced by the nature of the axial ligation to the iron, porphyrin peripheral substituents, solvent acces-

sibility of the metal site, electrostatic interactions with protein side chains and other cofactors, and protonation state of neighboring amino acids.

While the factors determining redox activity have been both experimentally and theoretically studied in natural heme proteins (3−8), de novo designed heme protein *maquettes*, synthetic protein scaffolds containing biochemical cofactors (9), offer a constructive approach to the study of the foundations of heme protein reduction midpoint potential control. In the present work, a family of water-soluble heme protein maquettes, synthetic four-α-helix bundles with heme-binding sites modeled after the cytochrome *b* subunit of the cytochrome bc_1 complex (10−13) have been constructed to incorporate various micro- and macroenvironmental factors. Using this series of maquettes, we investigate the magnitude of redox activity regulation in synthetic proteins by the factors of heme peripheral substitution, electrostatic interactions with charged amino acids in heme vicinity as well as with other heme cofactors, and protonation/deprotonation of neighboring amino acids (Figure 1). As a result, we achieve significant diversity in the heme reduction midpoint potential (435 mV) within our prototype synthetic heme protein maquette system.
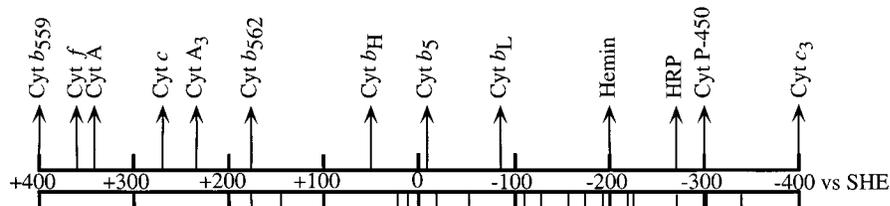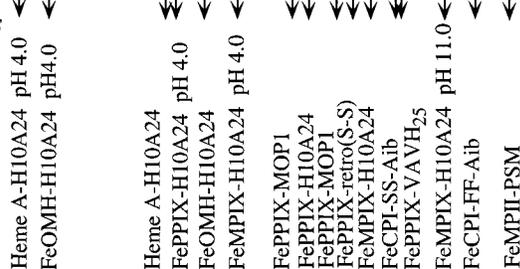
MATERIALS AND METHODS

Trifluoroacetic acid, diethyl ether, acetic anhydride, piperidine, and pyridine were obtained from the Aldrich

---

* Corrresonding author. Phone: (215)898-5668. Fax: (215)573-2235. E-mail: dutton@mail.med.upenn.edu.

[‡] Present address: Division of Biology, California Institute of Technology, 147-75, Pasadena, CA 19125.

[§] Present address: Department of Chemistry, Columbia University, New York, NY 10027.

Scheme 1:   Redox Activity Scale of Natural and Synthetic Cytochromes[a]

Natural Heme Proteins

Cyt b_{559}, Cyt f, Cyt A, Cyt c, Cyt A_3, Cyt b_{562}, Cyt b_H, Cyt b_5, Cyt b_L, Hemin, HRP, Cyt P-450, Cyt c_3

+400   +300   +200   +100   0   -100   -200   -300   -400 vs SHE

Synthetic Heme Proteins

Heme A-H10A24 pH 4.0, FeOMH-H10A24 pH4.0, Heme A-H10A24, FePPIX-H10A24 pH 4.0, FeOMH-H10A24, FeMPIX-H10A24 pH 4.0, FePPIX-MOP1, FePPIX-H10A24, FePPIX-MOP1, FePPIX-retro(S-S), FeMPIX-H10A24, FeCPI-SS-Aib, FePPIX-VAVH$_{25}$, FeMPIX-H10A24 pH 11.0, FeCPI-FF-Aib, FeMPII-PSM

[a] The reduction midpoint potential of free hemin, FePPIXCl, in aqueous solution is shown for comparison. Reduction midpoint potential values correspond to pH 7−8 range. References for redox activity values: cyt b_{559} (2), cytochrome f of cytochrome b_6f complex (57), cytochrome A and cytochrome A_3 of cytochrome c oxidase (28), cytochrome c (58), cytochrome b_{562}(59), cytochrome b_L and b_H of cytochrome bc_1 complex (60), cytochrome b_5 (61), horseradish peroxidase (62), cytochrome P-450 (63), TASP designed proteins di-FePPIX MOP1 (47), designed FePPIX proteins retro(S−S) and VAVH$_{25}$ (46), self-assembled peptide FeCPI-FF-Aib (51), peptide sandwiched mesoheme (FeMPIX-PSM) (52).

FePPIX$_2$-H10A24

Heme A

FeOMH
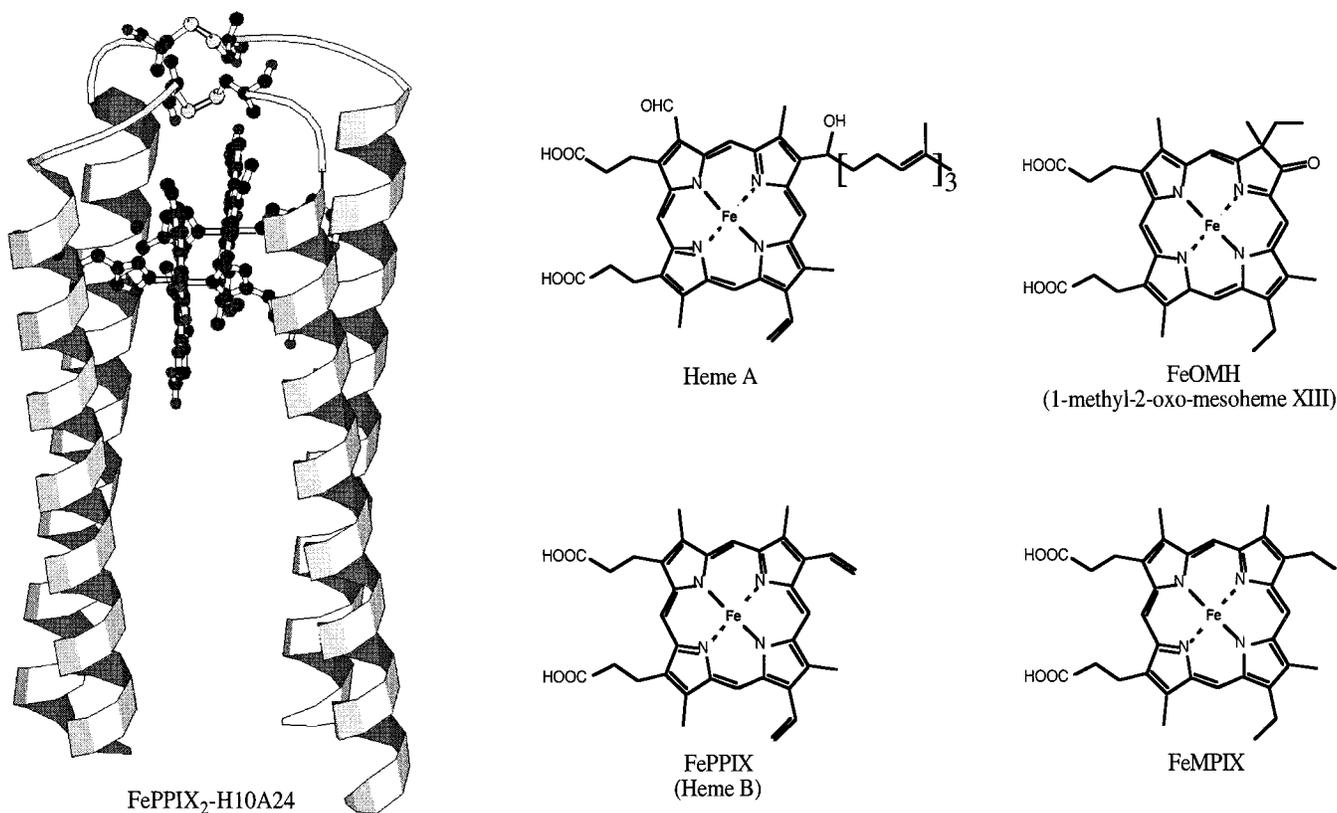(1-methyl-2-oxo-mesoheme XIII)

FePPIX
(Heme B)

FeMPIX

FIGURE 1: Molecular modeling representation of the FePPIX$_2$-H10A24 heme protein maquette and the various metalloporphyrins derivatives utilized in this study. Modeling was performed on a Silicon Graphics Indigo^2 workstation (Mountain View, CA) using SYBYL (Tripos Associates, St. Louis, MO).

Chemical Co. (Milwaukee, WI). Ethanedithiol and 1-hydroxybenzotriazole (HOBt)[1] were purchased from Fluka (Ronkonkoma, NY). Hemin was purchased from Porphyrin Products Inc. (Logan, UT). The NovaSyn PR-500 resin was purchased from Calbiochem-Novabiochem (La Jolla, CA). Natural Fmoc-protected amino acids were acquired as pentafluorophenyl esters from PerSeptive Biosystems (Framingham, MA) with the exception of Fmoc-L-Arg(Pmc)-OPfp, which was purchased from Bachem (King of Prussia, PA). Guanidine hydrochloride (8 M) was used as received from Pierce (Rockford, IL). Redox mediator dyes were purchased from Aldrich Chemical Co. (Milwaukee, WI) with the exception of pyocyanine, which was synthesized from N-methylphenazonium methosulfate obtained from Fluka (Ronkonkoma, NY). All other chemicals and solvents were reagent grade.

Protein Design and Assembly. The tetra-α-helix bundle design was based on the heptad repeat strategy where helical assembly is predominantly driven by the hydrophobic effect (*14−16*). The bundle core (heptad positions a, d, and e) is mostly comprised of hydrophobic leucines with phenylalanines and iron ligating histidines. The exterior of the bundle is composed of polar lysines (heptad positions f and g) and glutamates (heptad positions b and c) that confer water solubility to the peptide and potentially provide electrostatic stabilization of the bundle assembly. The peptides described in this work were synthesized as a 31-amino acid stretch that was subsequently homodimerized through the N-terminal cysteine to form a disulfide linked 62-amino acid peptide (α-ss-α). Histidine residues were placed at positions 10 (a positions of the heptad repeat) to provide the FePPIX iron with bis-histidine coordination. The basic synthetic bundle utilized in this work has the following sequence:

H10A24: (α-SH) Ac-CGGGELWKL·$\mathbf{H}^{10}$EEL^{13}LKK· FEELLKL·A^{24}EERLKK·L-CONH$_2$

The other peptides used are referred to throughout this work by the histidine sequence position followed by any other modifications as compared to the prototype sequences shown above. For example, H10A24-E11Q corresponds to a peptide with the sequence H10A24 and a glutamate at each position 11 substituted by a glutamine. All synthetic peptides described in this work spontaneously associate in aqueous solution to form noncovalent dimers designed to provide two bis-histidine metalloporphyrin binding sites. As dimers, the peptides can exist in one of two global topologies, syn (loop regions on the same end of the bundle) or anti (loops on opposite ends of the bundle). We have previously established that the two (α-ss-α) subunits of the H10A24 bundle assemble in the syn topology with adjacent metalloporphyrins (modeled Fe−Fe distance of 11 Å). Furthermore, the global topology of the two H10A24 subunits can be altered by single amino acid changes (H10S24) (*17*) or by porphyrin macrocycle incorporation (heme A$_2$-H10A24) (*18*). The global topology for maquettes studied may be variable depending on peptide sequence, number, and types of metalloporphyrins incorporated because the energetic differences between the global topologies are relatively small (2−4 kcal/mol) as compared to the measured global stabilities (>15 kcal/mol).

Peptide Synthesis. Each 31-amino acid peptide was synthesized by the solid-phase method on a continuous-flow MilliGen model 9050 synthesizer utilizing the Fmoc/^{t}Bu protection strategy. N-terminal acetylation of the peptides was performed with a 1:1 mixture of acetic anhydride/pyridine for 20 min prior to cleavage. The peptides were cleaved from the resins, and the amino acid side chain protecting groups were removed by exposure to a 90:8:2 (v: v:v) mixture of trifluoroacetic acid:ethanedithiol:water for 2 h. Crude peptides were precipitated with cold ether

followed by purification by reversed-phase C$_{18}$ HPLC with aqueous/acetonitrile gradients containing 0.1% trifluoroacetic acid. The peptides were homodimerized by oxidizing the N-terminal cysteine in air-saturated 100 mM ammonium bicarbonate buffer (pH 9) for 4 h. The purity of the disulfide-linked 62-amino acid (α-ss-α) peptides was characterized by analytical HPLC. The molecular mass of the purified peptides was verified by electrospray mass spectroscopy. Purified material was lyophilized and stored at −20 °C until use.

Solution Molecular Weight Determination. A Beckman System Gold HPLC pump and detector (Fullerton, CA) equipped with a Supelco GFC-100 column (7.5 × 300 mm, Sigma-Aldrich, Milwaukee, WI) equilibrated at a flow rate of 0.5 mL/min with 50 mM Tris-HCl and 100 mM NaCl pH 8.5 buffer was used for gel filtration chromatography. Column calibration was performed with a low molecular weight gel filtration calibration kit (Pharmacia Biotech, Uppsala, Sweden). Unless otherwise stated, the maquettes eluted with retention times consistent with a dimeric aggregation state, i.e., four helix bundle, with less than 10% of the material comprising higher oligomerization states.

Circular Dichroism. CD spectra were recorded on an Aviv Associates model 60DS spectropolarimeter using 0.2-cm quartz cuvette at 25 °C in 50 mM Tris-HCl and 100 mM NaCl pH 8.5 buffer. The peptide helicity was calculated from the CD absorbance at 222 nm (Θ_{222}) based on a 100% α-helix value of −32 000 deg cm^2 dmol^{-1} (*19*). The prototype H10A24 maquette contains 78% α-helix. Unless otherwise stated, all described peptides have approximately the same α-helical content.

Metalloporphyrin Incorporation into Peptides. The synthetic metalloproteins were prepared by incremental additions of 5-μL aliquots of a 1 mM solution of iron protoporphyrin IX or another specified metalloporphyrin in dimethyl sulfoxide (DMSO) to the peptide with gentle stirring (50 mM Tris-HCl and 100 mM NaCl pH 8.5 buffer) up to the desired metalloporphyrin/peptide stoichiometry. All the porphyrins studied exhibited binding affinities (0.1−50 nM range) for the first binding site in the H10A24 maquette and binding affinities for the second binding site of 0.8−5 μM. Binding of FePPIX, FeMPIX, and FeOMH to H10A24 was complete within 1 min. Since heme A binding to H10A24 shows slower kinetics, the sample was allowed to equilibrate for several hours (*18*). Samples of the monometalloporphyrin proteins were prepared by the addition of only 0.8 metalloporphyrin equiv per four helix bundle to avoid the presence of dimetalloporphyrin peptide species.

Bis-Imidazole-Ligated Metalloporphyrin Sample Preparation. For the study of bis-imidazole complexes of various natural and synthetic metalloporphyrins, samples were prepared by the addition of porphyrin solution in DMSO into the aqueous buffer (50 mM Tris-HCl and 100 mM NaCl, pH 8.5) to 5−10 μM porphyrin concentration. Then 2−3 M imidazole was added to drive formation of the bis-Im porphyrin species followed by adjustment of the pH to an appropriate value. This exact sequence of preparation is necessary to obtain nonaggregated bis-imidazole porphyrin complexes with UV−visible spectra characteristic of porphyrin monomers.

UV−Visible Spectroscopy. The spectra were recorded on a Perkin-Elmer Lambda 2 spectrophotometer. The peptide

---

[1] Abbreviations: ^{t}Bu, *tert*-butyl; DMSO, dimethyl sulfoxide; Fmoc, 9-fluorenylmethoxycarbonyl; HOBt, 1-hydroxybenzotriazole; HPLC, high-performance liquid chromatography; FePPIX, iron protoporphyrin IX; ZnPPIX, zinc-substituted protoporphyrin IX; FeMPIX, iron mesoporphyrin IX; FeOMH, iron 1-methyl-2-oxo-mesoheme XIII; (Im)$_2$, bis-imidazole complex; E_{mX}, equilibrium reduction midpoint potential at pH X; SHE, standard hydrogen electrode.

concentration was determined optically by the absorbance of the Trp (position 7 on each α-helix), using an extinction coefficient $\epsilon_{280} = 5600$ M^{-1} cm^{-1} (*20*). Fe(III)PPIX binding was monitored both by loss of absorption due to free hemin (385 nm) and by appearance of a prominent Soret band (412 nm), corresponding to Fe(III)PPIX bound to the protein via bis-histidine axial coordination.

Redox Titrations. Redox titrations were performed in combination with optical analysis, using the UV−visible spectrophotometer described above. Sample concentration was $5-15$ μM. The redox titrations were performed using an in-house designed glass redox cuvette with platinum measuring and calomel reference electrodes (Radiometer Analytical, Lyon, France) (*21*); the reported reduction midpoint potentials are referenced to a standard hydrogen electrode. All redox titrations were performed anaerobically using <1-μL additions of freshly prepared sodium dithionite to adjust the solution potential to more negative values and potassium ferricyanide to more positive values. The following redox mediators were used to stabilize the solution reduction potential: 20 μM duroquinone, 10 μM pyocyanine, 10 μM 2-hydroxy-1,4-naphthoquinone, 10 μM anthraquinone-2-sulfonate, 2 μM benzyl viologen, 1 μM phenylsafranine, and 1 μM indigocarmine.

Redox Titration Data Analysis. All of the FePPIX maquettes show a typical bis-histidine ligated FePPIX spectrum with a Soret maximum at 412 nm in the oxidized state. In the reduced state, the Soret band gains intensity, narrows, and shifts to 425 nm; the sharp α-band at 559 nm and β-band at 535 nm characteristic of bis-histidine ligated Fe(II)PPIX are evident in the reduced state. The positions of Soret, α- and β-bands varied for other studied metalloporphyrins. Redox titrations were always analyzed by monitoring the α- and Soret absorbance bands as the metalloporphyrin protein was reduced or oxidized. When one metalloporphyrin was incorporated in the bundle the data were analyzed using the Nernst equation:

$$\%R = \frac{1}{10^{(E_h - E_m)/(RT/nF)} + 1} \times 100 \qquad (1a)$$

The equation was modified when two metalloporphyrins were present:

$$\%R = \left(\frac{1/2}{10^{(E_h - E_{m1})/(RT/nF)} + 1} + \frac{1/2}{10^{(E_h - E_{m2})/(RT/nF)} + 1} \right) \times 100 \quad (1b)$$

where $\%R$ is percentage of reduced metalloporphyrin, E_h is the solution reduction potential versus the standard hydrogen electrode (SHE), n is the number of electrons participating in the redox reaction (fixed to 1.0 in all fittings) with E_{m1} and E_{m2} being the reduction midpoint potentials of interest. All potentiometric titrations were performed at 22 °C. When the data sets were fit allowing n to vary, n values of $0.9-1.1$ were routinely obtained with the exception of the potentiometric titration of FePPIX(Im)$_2$ which has a n value of 1.25. The high n value of FePPIX(Im)$_2$ may be due to sample heterogeneity due to incomplete coordinative saturation at the iron at the concentrations of imidazole used.

RESULTS

Effect of Metalloporphyrin Incorporation into the H10A24 Maquette on Iron E_m. As a starting point, we evaluated the
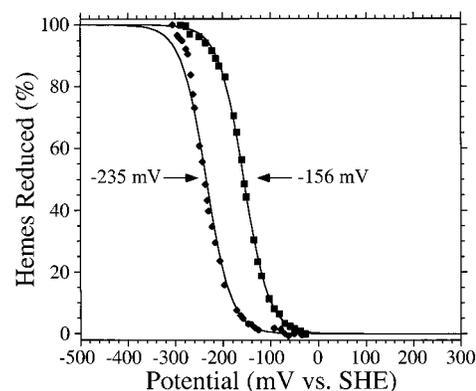

FIGURE 2: Comparison of the redox titrations of bis-imidazole-ligated FePPIX (filled diamonds) and the FePPIX-H10A24 maquette (filled squares) illustrating the effect of FePPIX incorporation into the peptide on the reduction midpoint potential at pH 8.5 ($E_{m8.5}$). The arrows indicate the reduction midpoint potentials obtained from fitting to eq 1a, −235 mV for FePPIX(Im)$_2$ and −156 mV for FePPIX-H10A24 vs SHE. Titrations were performed at 22 °C in pH 8.5 buffer (100 mM Tris-HCl, 50 mM NaCl).

effect of the peptide scaffold on the reduction potential of the various metalloporphyrins by comparing the E_m values within the H10A24 maquette to the corresponding bis-imidazole-ligated metalloporphyrins in isotropic aqueous solution. Figure 2 shows a comparison of the redox titrations of FePPIX(Im)$_2$ and FePPIX-H10A24 that reveals the extent to which incorporation of the FePPIX macrocycle into the protein core influences the reduction midpoint potential. FePPIX(Im)$_2$ in aqueous solution at pH 8.5 exhibits a reduction midpoint potential of −235 $\pm$ 15 mV; whereas, the $E_{m8.5}$ of FePPIX-H10A24 is raised to −156 $\pm$ 7 mV vs SHE. The approximately 80 mV (1.8 kcal/mol) increase in the FePPIX reduction midpoint potential from −235 to −156 mV upon binding to the H10A24 maquette demonstrates that the metalloporphyrin site is well protected from the solvent, surrounded by a low dielectric media that destabilizes the positively charged [Fe(III)PPIX]$^+$ with respect to the neutral Fe(II)PPIX, thereby raising iron reduction midpoint potential (*22*). Conversely, the highly polar and mobile aqueous solvent stabilizes the ferric state, lowering the solvent-exposed FePPIX(Im)$_2$ reduction potential.

Effect of Electron-Donating/Withdrawing Properties of Metalloporphyrin Substituents. The ability of various metalloporphyrin cofactors to accept or donate electrons is influenced by the electron-donating/accepting nature of peripheral porphyrin substituents, so that different types of metalloporphyrins display intrinsically different reduction potential values. To address the influence of different electron-donating and -withdrawing peripheral substituents on $E_{m8.5}$ within the same maquette scaffold, we compared the redox properties of FePPIX to that of other natural and synthetic metalloporphyrins. For this purpose, we have used FeMPIX (iron mesoporphyrin IX), the closest in structure to heme C of *c*-type cytochromes; heme A, present in the *a*-type cytochromes of the cytochrome *c* oxidase; and synthetically made FeOMH (iron 1-methyl-2-oxo-mesoheme XIII) (see Figure 1 for structures). The redox activity of those cofactors incorporated in H10A24 are summarized in Table 1. The $E_{m8.5}$ of FePPIX-H10A24 was measured as −156 $\pm$ 7 mV vs SHE. The conversion of the vinyl substituents on FePPIX into the ethyl substituents of FeMPIX results in a

Table 1: Comparison of Reduction Midpoint Potential Values for Different Heme Types in Bis-Imidazole Complex in Solution and Bound to the H10A24 Maquette

| | redox potential, mV vs SHE | | | |
| | | inside H10A24 maquette | | |
heme type	Bis-imidazole complex in aq solution	single heme, pH 8.5	single heme, pH 4.0	two hemes, pH 8.5
FePPIX	−235	−156	+5	−216, −144
FeMPIX	−285	−196	−55	−241, −177
heme A	−120[a]	+18	+170	−45, −45[b]
FeOMH	−48	−12	+143	

[a] Taken from ref *54*. [b] Taken from ref *18*.

monometalloporphyrin reduction potential of −196 ± 8 mV lowered by 40 mV relative to FePPIX due to the greater electron-donating capacity of the sp^3 hybridized carbons which stabilizes the ferric state. The incorporation of the formyl group of heme A, a strong electron-withdrawing substituent, results in a dramatic elevation of the $E_{m8.5}$ by >170 mV to +18 mV. The incorporation of an oxo group onto a porphyrin pyrrole ring in FeOMH raises the reduction potential of FeOMH-H10A24 to −12 mV again due to a strong electron-withdrawing effect, this time due to the oxo group. These results illustrate that the incorporation of electron-donating and -withdrawing porphyrin substituents can modulate the reduction potential by as much as 200 mV within a single maquette scaffold.

Comparing the reduction midpoint potentials of the electron-donating/withdrawing metalloporphyrins in their bis-imidazole-ligated forms and sequestered in H10A24 allows evaluation of the role of protein matrix in determining heme E_m. The reduction potential of FeMPIX(Im)$_2$ is 89 mV lower than that of FeMPIX-H10A24, consistent with the value measured for FePPIX, illustrating that incorporation of the metallomacrocycles into protein has a similar effect on E_m for these two related metalloporphyrins (Table 1). A greater effect is shown by heme A, whose E_m at +18 mV is raised by 138 mV relative to its bis-imidazole-ligated value. A diminished effect is demonstrated by FeOMH whose E_m is elevated by only 36 mV upon incorporation into H10A24. These results illustrate that while incorporation of the metalloporphyrin macrocycles into H10A24 in all cases raises the midpoint potentials relative to their respective bis-imidazole complexes, the exact magnitude of the elevation is variable between 40 and 140 mV.

Effect of Local Amino Acid Charges. We explored the role of electrostatic interactions in modulating the FePPIX redox activity of FePPIX-H10A24 by specifically introducing charged amino acids in close proximity to the metalloporphyrin binding site of H10A24. The effects were evaluated in the mono-FePPIX form to eliminate complications due to ferric FePPIX−ferric FePPIX electrostatic interactions at this site. Two variants of the H10A24 maquette were constructed with the leucine at position 13 (d position of the heptad repeat one helical turn down from heme-ligating histidine H10) replaced by a potentially negatively charged glutamic acid, H10A24-L13E, and a positively charged arginine, H10A24-L13R. In the third variant, a glutamate at position 11 (heptad b position) was substituted by a neutral but polar glutamine (H10A24-E11Q). All the variants assembled into four-α-helix bundles in aqueous solution with
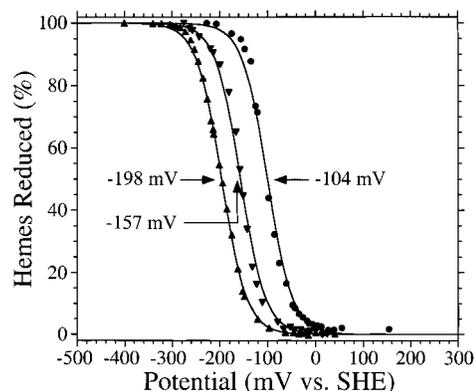

FIGURE 3: Potentiometric titrations of the charged variants of H10A24 demonstrating the effect of local charge placement on FePPIX electrochemistry: (filled triangles) FePPIX-H10A24-L13E, (filled inverted triangles) FePPIX-H10A24-L13R, and (filled circles) FePPIX-H10A24-E11Q are shown. The experimental conditions are the same as in Figure 2.

helicity unaltered for H10A24-E11Q (78%) but decreased to 74% in H10A24-L13R and to 63% in H10A24-L13E, consistent both with the lower helix propensities of Glu and Arg relative to Leu and the incorporation of polar residues into a interior heptad d position. Despite these minor changes in the apo state helical content, these peptides bind FePPIX tightly (K_{d1} in the 0.1−10-nM range), illustrating the robust nature of the H10A24 design.

Figure 3 compares the redox potentiometric titrations of the mono-FePPIX-incorporated charge variants of the H10A24 maquette. The replacement of a glutamate for a glutamine at position 11 in H10A24-E11Q raises the reduction midpoint potential by about 50 mV in comparison to that of the prototype H10A24 maquette consistent with the loss of stabilization of the [Fe(III)PPIX]$^+$ by the negatively charged Glu 11. The introduction of a glutamate at position 13, H10A24-L13E, lowers the ferric FePPIX reduction potential by 42 mV to −198 mV in agreement with the increased stabilization of the ferric FePPIX by the neighboring Glu 13. Contrary to expectations, substitution of an arginine at the same position yields a peptide, H10A24-L13R, with an unaltered redox activity of −157 ± 8 mV. The lack of response of the FePPIX reduction midpoint potential to a local arginine residue suggests that the guanidinium moiety is fully solvent exposed, as observed at the analogous heptad d position 27 in the NMR structure of [H10H24-L6I,L13F]$_2$ (*23−25*). These results illustrate that the FePPIX redox activity in H10A24 can be modulated by 40−50 mV via a local charged amino acid substitution; however, long flexible amino acid side chains that allow for exposure of the charged groups to solvent compromise the expected reduction midpoint potential shift.

Effect of Cofactor−Cofactor Interactions. The prototype H10A24 heme protein maquette is a homodimer known to assemble with the two (α-ss-α) subunits in a syn topology, i.e., loops at same end of the maquette (*17*). As such, two metalloporphyrins bind in adjacent sites, one in each (α-ss-α) subunit, with a modeled distance of 11 Å between the iron ions. The interaction between the two cofactors bound at the adjacent sites results in a pronounced splitting of their reduction midpoint potentials (*9*). The splitting has been attributed to the electrostatic repulsion between the [Fe(III)-
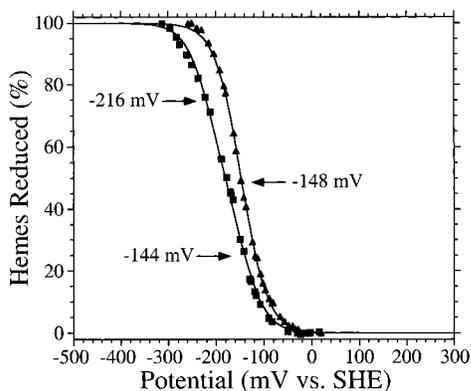
FIGURE 4: Redox titration of FePPIX$_2$-H10A24 (filled squares) compared with the mixed metalloporphyrin [ZnPPIX, FePPIX]-H10A24 (filled trianges) showing that the observed midpoint splitting in FePPIX$_2$-H10A24 results from the adjacent formally charged oxidized [Fe(III)PPIX]$^+$. Experimental conditions are as in Figure 2.

PPIX]$^+$ moieties that promotes reduction of one of the cofactors, raising its redox activity. Once one of the metalloporphyrins is reduced and formally neutral, the electrostatic interaction between cofactors is lost; hence, the potential of the second [Fe(III)PPIX]$^+$ is unperturbed by the presence of the first, already reduced cofactor.

We explored the presence of metalloporphyrin−metalloporphyrin electrostatic interactions within the protein maquettes using both FePPIX and the variant with the simplest modification, FeMPIX. Figure 4 shows the redox titration of the FePPIX$_2$-H10A24 maquette. The data require fitting to two separate reduction processes (eq 1b) yielding the reduction midpoint potential values of -144 ± 15 and -216 ± 15 mV vs SHE. The splitting of 72 mV between the cofactor potentials is in agreement with previous findings (*9*). However, the obtained values of reduction midpoint potentials for two sites in FePPIX$_2$-H10A24 are not as expected for such a simple model. The redox activity of the first FePPIX to be reduced in the FePPIX$_2$-H10A24 is slightly raised in comparison to the mono-FePPIX-H10A24 value (-156 mV), while the potential of the second site in the FePPIX$_2$-H10A24 maquette is lowered by 60 mV (Table 1). A similar situation to FePPIX$_2$-H10A24 is observed for the maquette incorporated with two FeMPIX cofactors, FeMPIX$_2$-H10A24 (Table 1). A splitting of 64 mV is evident; however, the reduction midpoint potential of the second FeMPIX to be reduced, -241 mV, is lowered by about 35 mV in respect to the single FeMPIX-H10A24 value of -196 mV.

Assignment of the reduction midpoint potential splitting observed in FePPIX$_2$-H10A24 and FeMPIX$_2$-H10A24 solely to electrostatic interactions between the ferric cofactors was made by study of the redox properties of H10A24 maquette simultaneously incorporated with an FePPIX and a Zn-substituted metalloporphyrin, ZnPPIX. ZnPPIX binds to maquettes with high binding affinity (nM) through a single histidine as a five-coordinated Zn species (*26*). Unlike FePPIX, ZnPPIX carries no formal charge and is electrochemically inactive in the potential range studied (from -400 to $+200$ mV). Figure 4 also gives the redox titration of [ZnPPIX,Fe(III)PPIX]-H10A24 which clearly corresponds to a single reduction process with E_m at -148 ± 12 mV, a value similar to FePPIX-H10A24 (-156 mV) and consistent

with the abolishment of electrostatic interaction between the cofactors. These results illustrate that the 72-mV modulation in FePPIX reduction midpoint potentials in the di-FePPIX maquettes with syn topology is due primarily to [Fe(III)-PPIX]$^+$−[Fe(III)PPIX]$^+$ electrostatic interactions.

Effect of Solution pH. Lowering the solution pH is known to increase the redox activities of many natural heme proteins in which FePPIX oxidation/reduction is coupled to proton binding/release (*27−34*). This redox-Bohr effect has been successfully reproduced in FePPIX protein maquettes (*35*) where lowering the pH from 11 to 4 produced a 210-mV elevation of the FePPIX-H10A24 reduction midpoint potential from -205 to $+5$ mV without significant changes to the four-α-helix bundle architecture. The majority of the observed increase, 160 mV, in the reduction midpoint potential value was attributed to abolishment of electrostatic stabilization of the ferric [Fe(III)PPIX]$^+$ upon protonation of a glutamate side chains, with Glu11 contributing 50 mV of the 160 mV total. Additionally, lysine residues contributed the $\approx$50 mV modulation observed above pH 8.0.

We investigated the effect of external solution pH on the redox properties of various metalloporphyrins incorporated into H10A24. Table 1 compares the equilibrium reduction midpoint potential values of different maquette-incorporated metalloporphyrins at pH 4.0, where the majority of glutamic acid side chains in the bundle are protonated (*35*), to those at pH 8.5, where the glutamates are known to stabilize the formally cationic ferric porphyrins. The data shows that lowering the pH by 4.5 units increases the redox activity of all the maquette-incorporated metalloporphyrins by $\approx$160 mV (3.7 kcal/mol). These results illustrate that the external pH can modulate the reduction potential by as much as 160 mV and that the partial charge compensation of the heme by glutamates is independent of the metalloporphyrin peripheral substituents.

DISCUSSION

We have examined the effect of various factors on the equilibrium reduction midpoint potential of iron porphyrins bound to four-α-helix bundle heme protein maquettes. By systematically examining various interactions within a single maquette scaffold, we are able to rank these interactions according to the magnitude of the E_m modulation. Additionally, we delineated which effects could be combined in tandem to yield predictable control of the resulting E_m values. Scheme 1 shows that we can modulate the iron porphyrin midpoint potential by some 435 mV or $\approx$10 kcal/mol (comparing heme A-H10A24, pH 4.0, at $+170$ mV to FeMPIX-H10A24, pH 11, at -265 mV) encompassing fully half the range observed in natural cytochromes.

The largest effect at $\approx$225 mV was observed for the electron-withdrawing/donating metalloporphyrin peripheral substituents. This might be as expected since these groups are in direct electronic communication with the encapsulated iron via covalent bonds. Changing the electron-donating capacity of the pyrrole nitrogens results in significant changes in the reduction potential of the iron ion. Similarly, the various iron coordination spheres observed in natural proteins can modulate the E_m by at least 400 mV since these changes alter the nature of the axial ligation at the iron. While de novo designed heme proteins rarely access ligation motifs

other than bis-His, their utilization in the future should allow for further modulation of the midpoint potential.

Second in magnitude to the metalloporphyrin substituents is the effect of solution pH. The 160 mV shift in the E_m of FePPIX-H10A24 between pH 4.0 and pH 8.5 can be transferred to the other iron porphyrins studied, illustrating a generalized and metalloporphyrin-type independent mechanism of proton-coupled redox reaction in maquettes. This effect can also be transferred to related maquette scaffolds with altered hydrophobic cores, as FePPIX-H10F24-L6I,L13F shows an identical 160 mV shift in E_m between pH 4.5 and pH 8.5 due to identical pK_a values although the reduction potentials are 50 mV lower (*36*). These results indicate that the pH dependence is a direct result of the -KLHEE- sequence local to each of these H10A24 iron porphyrin binding sites.

The third strongest effector of metalloporphyrin reduction potential was sequestration of the macrocycle by the hydrophobic core of the peptides. While incorporation of a cofactor into peptides has always resulted in an increased iron reduction midpoint potential, the magnitude of the increase was variable among the metalloporphyrins studied. The variability in this factor may be due to differences in the extent to which the macrocycle inserts into the hydrophobic core, since changes as small as 4 $Å^2$ in *c*-type cytochrome macrocylce solvent accessibility can have a 50-mV effect (*37*). The farnesyl side chain of heme A may drive the macrocycle further into the core in heme A-H10A24 or perhaps protect the heme A edge from solvent exposure, either way destabilizing the formally charged ferric state to a greater degree, raising the E_m by 138 mV. The similarity between FePPIX and FeMPIX suggests that these two related metalloporphyrins insert in a similar manner and to a lesser extent than heme A. Finally, the oxo unit on FeOMH, which makes it less hydrophobic than FePPIX perhaps allows it to expose a greater portion of the macrocycle to the high dielectric solution, which lowers the effect of incorporation into the peptide to 36 mV. While this factor is variable, its use in concert with solution pH renders the effect predictable.

Single charge substitutions near the iron porphyrin binding site, amino acid or metalloporphyrin based, modulate the E_m of the iron bound to H10A24 by a variable amount. The incorporation of negative charges in H10A24-L13E lowers the redox activity by ≈40 mV (−198 mV for FePPIX-H10A24-L13E vs −156 mV for FePPIX-H10A24) while elimination of the proton coupling glutamate in H10A24-E11Q raises the equilibrium reduction midpoint potential by ≈50 mV at pH 8.5 to −104 mV. The values are similar to those observed in natural heme proteins: cytochrome *c* (*38*–*40*), cytochrome b_5 (*41*), cytochrome *c* peroxidase (*42*), cytochrome c_2 (*43*), and the cytochrome bc_1 complex (*44*). However, the H10A24-L13R modification that results in no measurable change in the iron E_m value illustrates that charge modifications sometimes produce unexpected results, as the preference for solvation of the charged group and its flexibility may drive it from the hydrophobic core and reduce its efficacy.

The effect of the adjacent oxidized [Fe(III)PPIX]$^+$ is also somewhat variable within di-FePPIX maquette scaffolds ranging from 65 to 130 mV depending on the local amino acid sequence (*36*). Two FePPIX in the prototype H10A24 maquette in a syn topology exhibit a 70-mV splitting of the

reduction potentials independent of the metalloporphyrin architecture studied. Whereas in an anti topology, induced by either an insertion of a serine at the a position in H10A24-A24S (*17*) or by addition of two bulky hemes A (*18*), this splitting is abolished. Since the redox activity of the second site in FePPIX$_2$-H10A24 is about 50 mV lower than the mono-FePPIX-H10A24 value, it appears to disagree with the simple electrostatic destabilization model proposed. However, it could be explained by changes in the structure of the bundle associated with single or multiple cofactor binding. The recently available NMR structural data for H10H24-L6I,-L13F in the apo form (*23, 24*) suggests a necessity for such changes upon the incorporation of either metalloporphyrin macrocycle into the maquette, as no formal cavity exists within the tightly packed hydrophobic core of the apo state. Since our results suggest that the apo, mono-FePPIX, and di-FePPIX forms of the maquettes are structurally distinct, it is likely that more complete burial of the cofactor is possible in FePPIX-H10A24 than in FePPIX$_2$-H10A24 based on simple steric factors. Accommodating two iron porphyrins into the maquette forces greater solvent exposure of both cofactors as compared to the mono-FePPIX state leading to the lower reduction midpoint potential values observed (*22*). Additionally, the E_m value measured for the [ZnPPIX,-FePPIX]-H10A24 maquette (−148 mV) indicates that FePPIX remains as well protected from the solvent as a single FePPIX in FePPIX-H10A24, indicating that the alternative coordination of ZnPPIX at the adjacent site does not interfere with macrocycle burial.

Single hydrophobic amino acid substitutions local to the heme binding site can have a 50-mV effect on the FePPIX reduction midpoint potential in maquettes. Recently, Gibney et al. (*36*) have illustrated that either of two modifications of H10A24F, L6I or L13F, results in a 48-mV drop in the mono-FePPIX reduction potential to −204 mV, relative to FePPIX-H10A24, and their combination, H10A24F,L6I,-L13F, lowers the reduction potential by 54 mV rather than by 96 mV (2 × 48 mV). Thus, single conservative hydrophobic amino acid can modulate the FePPIX E_m by ≈50 mV, and the effects appear not to be additive. Finally, it should be noted that the relative orientation of the helices within the four-α-helix bundle has no effect on the resulting midpoint potentials as long as the local constellation of amino acids is kept constant (*25*).

The number of synthetic metalloporphyrins binding proteins based on helical peptide structural motifs reported in the literature is growing rapidly and may offer insight into global trends in iron porphyrin reduction potentials (*45*). Since the majority of the existing designs to date utilize bis-histidine coordination of the iron porphyrin moiety, a direct comparison of the iron reduction midpoint potentials within different synthetic systems offers insight into the contributions of amino acid composition and protein architecture to the metalloporphyrin redox activity (Scheme 1).

In the initial designed FePPIX-binding proteins of De-Grado and co-workers, VAVH$_{25}$ and retro(S−S), containing single FePPIX cofactors attached between two helices diagonally opposed across four-α-helix bundles (*46*), the reduction midpoint potentials, $E_{m7.5}$, were measured to be −220 and −170 mV, respectively. More recently, a template-assembled di-FePPIX four-α-helix bundle design by Rau et al., MOP1, similar to H10A24 displayed reduction midpoint

potential values, $E_{m7.0}$, of −106 and −170 mV for the two FePPIX cofactors (*47*). All of these values are in the range displayed by the protein maquettes that may be due to their similar sequences and helical architectures. On the basis of DeGrado's alpha series (*48*), each of these four-α-helix bundles contains the exact sequence -LHE- local to the metalloporphyrin binding histidines. Thus, each possesses the charge compensating glutamate residue (Glu11 of H10A24), suggesting that each may have similar proton-coupled redox reactions. The slightly smaller VAVH$_{25}$ and retro(S−S) peptides relative to H10A24 and MOP1 suggest that the overall size of the four-α-helix bundle has little or no effect on determining the reduction potential of the bound FePPIX in these stable architectures.

Smaller peptide systems, like Benson's peptide-sandwiched-mesohemes containing modified FeMPIX (*49, 50*) and Suslick's self-assembly Fe-coproporphyrin I-peptide complexes (*51*), with a single iron porphyrin group bound between two minimal α-helices axially coordinated by histidine side chains, display significantly lower reduction potentials than the four-α-helix bundle architecture. While the lower reduction midpoint potentials of Benson's PSMs, measured to be in the range between −270 and −332 mV (*52*), are similar to or lower than bis-imidazole FeMPIX at −235 mV, they also show up to 60 mV of modulation due to local hydrophobic amino acids. Such hydrophobic modulation has also been shown by Suslick in a self-assembling metalloporphyrin-peptide system where Fe-coproporphyrin I, bis-imidazole complex with an E_m of −214 mV was incorporated and exhibited an E_m value range from −218 to −304 mV. The observed negative E_m modulation upon porphyrin incorporation into the above peptides is unlike the positive modulation seen in our maquettes, indicating that the protein matrix can affect the E_m value in both ways and this effect is sequence dependent.

Two potential mechanisms for raising the midpoint potential of the FePPIX maquettes that have currently not been successful are their insertion into a membrane, effectively lowering the dielectric constant, and the use of ligation motifs other than bis-histidine. An examination of natural proteins reveals that many of the high potential cytochromes *b* such as cytochrome b_{559} reside in membranes. Clearly, the H10A24 maquette with heme A incorporated has a midpoint potential of 18 mV some 300 mV lower than the natural cytochrome A of cytochrome *c* oxidase, a membrane protein. This may indicate that water-soluble four-α-helix bundle protein scaffolds can only provide the heme A group with limited protection from the high dielectric solvent. Additionally, the design of iron porphyrin ligation motifs that stabilize the ferrous state relative to the ferric state should raise the maquette E_m values substantially, e.g., +150−220 mV for His-Met (*1, 53−55*). Thus, achieving the full range of 800 mV observed in natural proteins may require future alterations in our maquette scaffold architectures. Nevertheless, by employing several modifications in combination (electron-withdrawing porphyrins at low pH), we can cover half the physiological range within a simple maquette scaffold.

In conclusion, the redox activity of a bis-histidine-ligated iron porphyrins within a water-soluble four-α-helix bundle at neutral pH is expected to lie between −50 and −300 mV. The contributions of specific amino acids to the determination of reduction midpoint potential in maquettes is rather modest. Greater modification of heme redox activity can be achieved through changes in protein architecture, heme peripheral substituents, and the protonation states of multiple ionizable amino acids. The success in accomplishing great diversity of metalloporphyrin reduction midpoint potential values in maquettes signals the near-future design of proteins with a predetermined reduction midpoint potentials for the construction of functional bioenergetic machines from first principles.

REFERENCES

1. Dolla, A., Florens, L., Bianco, P., Haladjian, J., Voordouw, G., Forest, E., Wall, J., Guerlesquin, F., and Bruschi, M. (1994) *J. Biol. Chem. 269* (9), 6340−6346.
2. Horton, P., Whitmarsh, J., and Cramer, W. A. (1976) *Arch. Biochem. Biophys. 176*, 244−247.
3. Moore, G. R., and Williams, R. J. P. (1977) *FEBS Lett. 79*, 229−232.
4. Gunner, M. R., and Honig, B. (1990) in *Electrostatic Analysis of the Midpoints of the Four Hemes in the Bound Cytochrome of the Reaction Center of Rp. Viridis* (Jortner, J. A. P. B., Ed.) Kluwer Academic Publishers, Amsterdam.
5. Gunner, M. R., and Honnig, B. (1991) *Proc. Natl. Acad. Sci. U.S.A. 88*, 9151−9155.
6. Churg, A. K., and Warshel, A. (1986) *Biochemistry 25*, 1675−1681.
7. Gunner, M. R., Alexov, E., Torres, E., and Lipovaca, S. (1997) *J. Biol. Inorg. Chem. 2*, 126−134.
8. Mauk, A. G., and Moore, G. R. (1997) *J. Biol. Inorg. Chem. 2*, 119−125.
9. Robertson, D. E., Farid, R. S., Moser, C. C., Urbauer, J. L., Mulholland, S. E., Pidikiti, R., Lear, J. D., Wand, A. J., DeGrado, W. F., and Dutton, P. L. (1994) *Nature 368*, 425−432.
10. Kim, H., Xia, D., Yu, C.-A., Xia, J.-Z., Kachurin, A. M., Zhang, L., Yu, L., and Deisenhofer, J. (1998) *Proc. Natl. Acad. Sci. U.S.A. 95*, 8026−8033.
11. Zhang, Z., Huang, L., Shulmeister, V. M., Chi, Y. I., Kim, K. K., Hung, L. W., Crofts, A. R., Berry, E. A., and Kim, S. H. (1998) *Nature 392*, 677−684.
12. Xia, D., Yu, C.-A., Kim, H., Xia, J.-Z., Kachurin, A. M., Zhang, L., Yu, L., and Deisenhofer, J. (1997) *Science 277*, 60−66.
13. Iwata, S., Lee, J. W., Okada, K, Lee, J. K., Iwata, M., Rasmussen, B., Link, T. A., Ramaswamy, S., and Jap, B. K. (1998) *Science 281*, 64−71.
14. DeGrado, W. F., Wasserman, Z. R., and Lear, J. D. (1989) *Science 243*, 622−628.
15. Hodges, R. S. (1996) *Biochem. Cell Biol. 74*, 133−154.
16. Betz, S. F., Bryson, J. W., and DeGrado, W. F. (1995) *Curr. Opin. Struct. Biol.* 457−463.
17. Grosset, A. M., Gibney, B. R., Rabanal F., Moser, C. C., and Dutton, P. L. (manuscript in preparation).
18. Gibney, B. R., Isogai, Y., Reddy, K. S., Rabanal, F., Grosset, A. M., Moser, C. C., and Dutton, P. L. *Biochemistry* (2000) *39*, 5683−5690.
19. Pace, C. N., Shirley, B. A., Thompson, J. A. (1989) in *Protein Structure: A Practical Approach* (Creighton, T. E., Ed.) IRL, Oxford.
20. Edelhoch, H. (1967) *Biochemistry 6*, 1948−1954.
21. Dutton, P. L. (1978) *Methods Enzymol. 54*, 411−435.
22. Stellwagen, E. (1978) *Nature 275*, 73−74.
23. Skalicky, J. J., Bieber, R. J., Gibney, B. R., Rabanal, F., Dutton, P. L., and Wand, A. J. (1998) *J. Biomol. NMR 11*, 227−228.

24. Skalicky, J. J., Gibney, B. R., Rabanal, F., Bieber-Urbauer, R. J., Dutton, P. L., and Wand, A. J. (1999) *J. Am. Chem. Soc. 121*, 4941−4960.

25. Gibney, B. R., Rabanal, F., Skalicky, J. J., Wand, A. J., and Dutton, P. L. (1999) *J. Am. Chem. Soc. 121*, 4952−4960.

26. Sharp, R. E., Diers, J. R., Bocian, D. F., and Dutton, P. L. (1998) *J. Am. Chem. Soc. 120*, 7103−7104.

27. Wilson, D. F., Lindsay, J. G., and Brocklehurst, E. S. (1972) *Biochim. Biophys. Acta 256*, 277−286.

28. Blair, D. F., Ellis, W. R., Jr., Wang, H., Gray, H. B., and Chan, S. I. (1986) *J. Biol. Chem. 261*, 11524−11537.

29. Petty, K. M., and Dutton, P. L. (1976) *Arch. Biochem. Biophys. 172*, 335−345.

30. Leitch, F. A., Moore, G. R., and Pettigrew, G. W. (1984) *Biochemistry 23*, 1831−1838.

31. Moore, G. R., Pettigrew, G. W., Pitt, R. C., and Williams, R. J. P. (1980) *Biochim. Biophys. Acta 590*, 261−271.

32. Moore, G. R., Williams, R. J., Peterson, J., Thomson, A. J., and Mathews, F. S. (1985) *Biochim. Biophys. Acta 829*, 83−96.

33. Costa, H. S., Santos, H., Turner, D. L., and Xavier, A. V. (1992) *Eur. J. Biochem. 208*, 427−433.

34. Saraiva, L. M., Liu, M. Y., Payne, W. J., Legall, J., Moura, J. J., and Moura, I. (1990) *Eur. J. Biochem. 189*, 333−341.

35. Shifman, J. M., Moser, C. C., Kalsbeck, W. A., Bocian, D. F., and Dutton, P. L. (1998) *Biochemistry 37*, 16815−16827.

36. Gibney, B. R., Huang, S. S., Skalicky, J. J., Fuentes, E. J., Wand, A. J., and Dutton, P. L. (manuscript in preparation).

37. Tezcan, F. A., Winkler, J. R., and Gray, H. B. (1998) *J. Am. Chem. Soc. 120*, 13383−13388.

38. Cutler, R. L., Davies, A. M., Creighton, S., Warshel, A., Moore, G. R., Smith, M., and Mauk, A. G. (1989) *Biochemistry 28*, 3188−3197.

39. Davies, A. M., Guillemette, J. G., Smith, M., Greenwood, C., Thurgood, A. G. P., Mauk, A. G., and Moore, G. R. (1993) *Biochemistry* 5431−5435.

40. Caffrey, M. S., and Cusanovich, M. A. (1994) *Biochim. Biophys. Acta 1187*, 277−288.

41. Rodgers, K. K., and Sligar, S. G. (1991) *J. Am. Chem. Soc. 113*, 9419−9421.

42. Bujons, J., Dikiy, A., Ferrer, J. C., Banci, L., and Mauk, A. G. (1997) *Eur. J. Biochem. 243*(1−2), 72−84.

43. Caffrey, M. S., and Cusanovich, M. A. (1991) *Arch. Biochem. Biophys. 2*, 227−230.

44. Gennis, R. B., Barquera, B., Van Doren, S. R., Arnaud, S., Crofts, A. R., Davidson, E., Gray, K. A., and Daldal, F. (1993) *J. Bioenerg. Biomembr. 25*, 195−209.

45. Gibney, B. R., and Dutton, P. L. (2001) in *Advances in Inorganic Chemistry* (Mauk, A. G., and Sykes, A. G., Eds.) Vol. 51, pp 409−455, Academic Press, New York.

46. Choma, C. T., Lear, J. D., Nelson, M. J., Dutton, P. L., Robertson, D. E., and DeGrado, W. F. (1994) *J. Am. Chem. Soc. 116*, 856−865.

47. Rau, H. K., and Haehnel, W. (1998) *J. Am. Chem. Soc. 120*, 468−476.

48. Ho, S. P., and DeGrado, W. F. (1987) *J. Am. Chem. Soc 109*, 6751.

49. Benson, D. R., Hart, B. R., Zhu, X., and Doughty, M. B. (1995) *J. Am. Chem. Soc. 117*, 8502−8510.

50. Arnold, P. A., Shelton, W. R., and Benson, D. R. (1997) *J. Am. Chem. Soc. 119*, 3181−3182.

51. Huffman, D. L., Rosenblatt, M. M., and Suslick, K. S. (1998) *J. Am. Chem. Soc.* 6183−6184.

52. Kennedy, M. L., Gibney, B. R., Dutton, P. L., Rodgers, K. R., and Benson, D. R. (manuscript in preparation).

53. Harbury, H. A., Cronin, J. R., Fanger, M. W., Hettinger, T. P., Murphy, A. J., Myer, A. P., and Vinogradov, S. N. (1965) *Proc. Natl. Acad. Sci. U.S.A. 54*, 1658−1664.

54. Raphael, A. L., and Gray, H. B. (1989) *Proteins 6* (3), 338−340.

55. Mus-Veteau, I., Dolla, A., Guerlesquin, F., Payan, F., Czjzek, M., Haser, R., Bianco, P., Haladjian, J., Rapp-Giles, B. J., Wall, J. D., et al. (1992) *J. Biol. Chem. 267* (24), 16851−16858.

56. Vanderkooi, G., and Stotz, E. (1965) *J. Biol. Chem.* 241, 3316−3323.

57. Metzger, S. U., Cramer, W. A., and Whitmarsh, J. (1997) *Biochim. Biophys. Acta 1319* (2−3), 233−241.

58. Clark, W. M. (1960) *Oxidation Reduction of Organic Systems*, Williams and Wilkins, Baltimore, MD.

59. Barker, P. D., Nerou, E. P., Cheesman, M. R., Thomson, A. J., de Oliveira, P., and Hill, H. A. O. (1996) *Biochemistry 35*, 13618−13626.

60. Rich, P. R., Jeal, A. E., Madgwick, S. A., and Moody, A. J. (1990) *Biochim. Biophys. Acta 1018*, 29−40.

61. Bagby, S., Barker, P. D., Guo, L.-H., and Hill, A. O. (1990) *Biochemistry 29*, 3213−3219.

62. Meunier, B., Rodriguez-Lopez, J. N., Smith, A. T., Thorneley, R. N., and Rich, P. R. (1998) *Biochem. J. 330*, 303−309.

63. Sligar, S. G., Cinti, D. L., Gibson, G. G., and Schenkman, J. B. (1979) *Biochem. Biophys. Res. Commun. 90*, 925−932.